COMMUNICATION

Narrow carbonyl resonances in proton-diluted proteins facilitate NMR assignments in the solid-state

Rasmus Linser · Uwe Fink · Bernd Reif

Abstract HNCO/HNCACO type correlation experiments are an alternative for assignment of backbone resonances in extensively deuterated proteins in the solid-state, given the fact that line widths on the order of 14–17 Hz are achieved in the carbonyl dimension without the need of high power decoupling. The achieved resolution demonstrates that MAS solid-state NMR on extensively deuterated proteins is able to compete with solution-state NMR spectroscopy if proteins are investigated with correlation times τ_c that exceed 25 ns.

Keywords Perdeuteration ·
MAS solid-state NMR spectroscopy · Micro-crystalline ·
PRE · Proton detection

Introduction

Nuclear Magnetic Resonance has become one of the major techniques for investigation of protein structure and function. In contrast to X-ray crystallography, NMR can also be used to investigate protein dynamics and does not rely on the availability of single crystals. For non-soluble species like membrane proteins (Lange et al. 2006) or fibrillar structures (Wasmer et al. 2008), MAS (Magic Angle Spinning) solid-state NMR is more and more becoming a powerful complementary technique to solution-state NMR. In the solid state, the line width depends on factors like sample homogeneity, MAS frequency and the efficiency of homo- and heteronuclear decoupling. The tumbling correlation time and thus the molecular weight of the protein is of no importance, as internal dynamics, which are responsible for relaxation, are independent of the size of the molecule. This allows to achieve narrow lines for large proteins in the crystalline state (Tian et al. 2009) as well as in tumbling impaired solutions (Mainz et al. 2009). Using highly deuterated proteins, we obtain line widths for ^1H and ^{15}N which are on the order of 20 and 10 Hz, respectively (Chevelkov et al. 2006). In comparison to standard solid-state NMR experiments carried out on protonated samples, the achieved heteronuclear line width in case of a perdeuterated protein is not dependent on the efficiency of high power decoupling. Triple resonance experiments involving a proton dimension for detection thus become more and more routine in solid-state NMR (Linser et al. 2008, 2009; Schanda et al. 2009; Zhou et al. 2007). Conventional assignment strategies in the solid-state rely on resolved ^{15}N chemical shifts (Baldus 2002; Pauli et al. 2001). Introducing a second chemical shift dimension facilitates resolving chemical shift degeneracies. Extensive deuteration is achieved by crystallizing the perdeuterated protein in a buffer which contains H_2O and D_2O in a ratio of around 10–30% (Akbey et al. 2009; Chevelkov et al. 2006).

Materials and methods

We used a perdeuterated sample of the SH3 domain of chicken α-spectrin, which was obtained by recombinant protein expression and purified as described previously (Chevelkov et al. 2007). Crystallization was induced in a buffer by a pH-shift from 3.5 to 7.5. To achieve a high degree of deuteration, the crystallization buffer contained H_2O and

R. Linser · U. Fink · B. Reif (✉)
Leibniz-Institut für Molekulare Pharmakologie (FMP),
Robert-Rössle Str. 10, 13125 Berlin, Germany
e-mail: reif@fmp-berlin.de

B. Reif
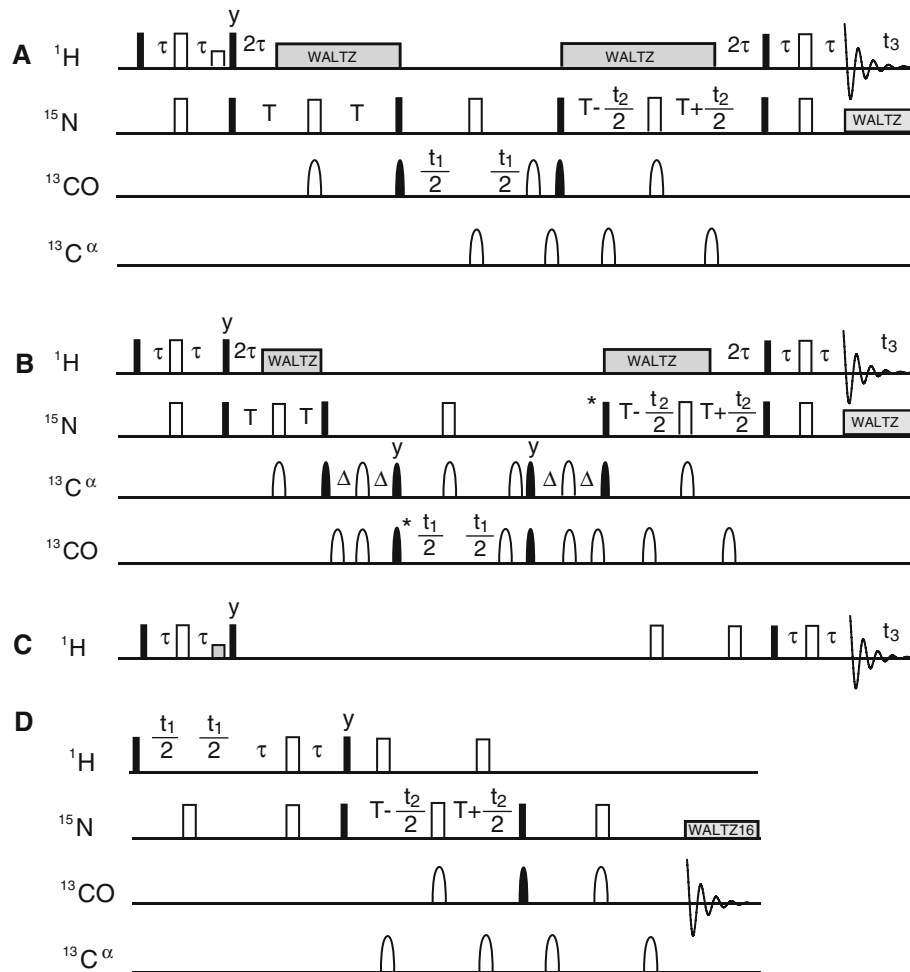Charité Universitätsmedizin, 10115 Berlin, Germany

Fig. 1 a Pulse sequence for the ^{1}H detected HNCO experiment. *Open bars* refer to 180° pulses, closed ones to 90° pulses. *Rectangular* and *curved bars* refer to hard and shaped pulses, respectively. **b** Pulse sequence for the ^{1}H detected HNCACO experiment. The ^{13}C carrier frequency was switched from C^α to CO directly before and after the t_1 evolution period. Selective on-resonance pulses on the ^{13}C channel were executed as soft rectangular pulses. Off-resonance selective pulses were implemented using G3 Gaussian cascade shapes (Emsley and Bodenhausen 1989; Emsley and Bodenhausen 1990). Pulses labeled with an asterisk were incremented according to TPPI. τ, T, and Δ were set to 2.5, 12, and 4 ms, respectively. **c** Alternative ^{1}H pulses for pulse schemes that use 180° pulses instead of Waltz-16 for scalar decoupling. The phase of the 2nd and 3rd 90° ^{15}N pulse are changed by 90°. Otherwise, the pulse scheme is executed as indicated in (**a** and **b**). The open bar with reduced height refers to a 1 ms purge pulse for water suppression. **d** Pulse sequence for the *J*-based ^{13}C detected HNCO experiment used to obtain the ^{13}C-1D spectrum represented for comparison in Fig. 3b

D_2O in a ratio of 1:9. We employed Paramagnetic Relaxation Enhancement (PRE) with 150 mM Cu(edta) for acceleration of data acquisition (Linser et al. 2007). After precipitation overnight, crystals were spun into a 3.2 mm rotor using approximately 15 mg protein. All NMR experiments were carried out on a Bruker Biospin AVANCE spectrometer operating at a ^{1}H Larmor frequency of 600 MHz, using a 3.2 mm triple-resonance probe. The MAS frequency was adjusted to 24 kHz. The acquisition time in the ^{15}N dimension in the triple resonance experiments was $t_2^{max} = 22$ ms. The effective temperature in the HNCO and HNCOCA was set to ~ 22°C. For the HNCACO correlation in Fig. 2, a temperature of 4°C was used. Data processing was performed using Bruker Topspin and Sparky (Goddard and Kneller). Apodization in the direct and indirect dimension was achieved by application of exponential multiplication using 10 Hz line broadening and gaussian multiplication using a line broadening of −10 Hz and a shift of the bell by 0.1, respectively.

Results and discussion

Complementary to the standard HNCA/HNCACB suite of experiments for assignment (Linser et al. 2008), we suggest to employ HNCO and HNCACO type experiments (Clubb et al. 1992; Engelke and Rüterjans 1995) to make use of the well-resolved H^N, N, and CO_{i-1}/CO_i resonances and the

excellent resolution in the carbonyl dimension. Figure 1 shows the pulse sequences that we employ to record HNCO (A) and HNCACO (B). The scheme represented in (C) uses 180° pulses to achieve proton scalar decoupling during the back-transfer from nitrogens to protons instead of the composite pulse sequence Waltz-16 (Shaka et al. 1983).

In combination with HNCACB type experiments, the use of carbonyl chemical shifts increases the reliability of the backbone assignments in the solid-state. A representative strip plot aligning inter- and intraresidual correlations for residues 9–18 in the α-spectrin SH3 domain is depicted in Fig. 2.

A 3D HNCO can be recorded in a few hours. An HNCACO with good signal to noise ($\sim$25:1 for CO_i, recycle delay 530 ms) can be recorded within 3 days. Correlations to CO_{i-1} appear with a peak intensity of about 2/3 in comparison to the CO_i peak intensity. In the HNCACO, all of the assigned residues yield two correlations, except for L8, E22, N35, V46, R49 and S36, Q50, D62, for which we only find one and no correlation peak, respectively. Similarly, HNCOCA correlations can be recorded with the same pulse scheme, in which pulses on the C^α channel are exchanged with pulses on the CO channel (Fig. 3).

CO resonances yield an improved dispersion in comparison to C^α due the fact that homonuclear scalar decoupling is easily achieved in the carbonyl dimension. Figure 4a shows the first 2D ^{1}H,^{13}CO plane extracted from
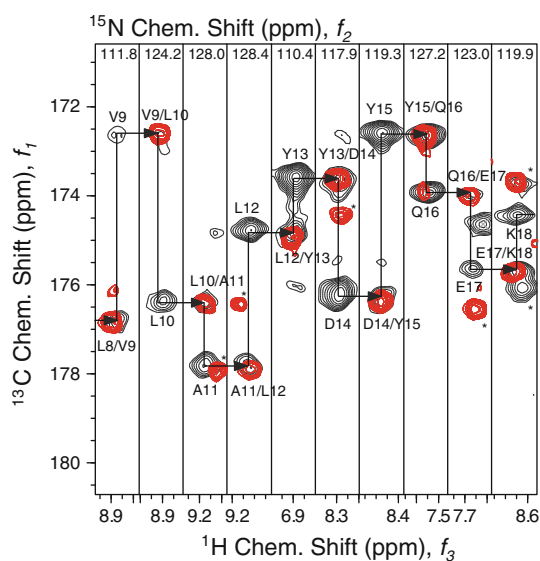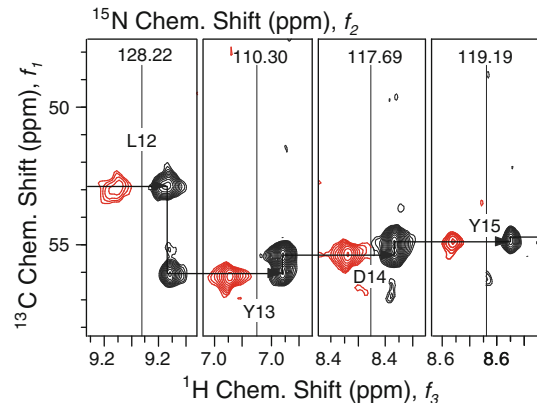
Fig. 3 Strip plots of the MAS solid-state NMR HNCOCA experiment showing residues L12-Y15 from the α-spectrin SH3 domain. Sequential correlations can be obtained via the HNCA experiment (black). Unambiguous assignment is facilitated using the HNCOCA experiment (red), which exclusively yields interresidual H_i^N-N_i^H-C_{i-1}^α correlations. This experiment is complementary to the HNCA experiment, in which the intraresidual H_i^N-N_i^H-C_i^α correlation is more pronounced

a 3D HNCO experiment. Typically, we find line widths on the order of 14–17 Hz for the carbonyl resonance. Importantly, this resolution is achieved without heteronuclear decoupling and therefore represents an upper limit for the achievable resolution. In contrast, the effective C^α line widths are typically on the order of 100 Hz due to evolution of ^{13}C,^{13}C homonuclear and ^{2}H,^{13}C$^\alpha$ heteronuclear scalar couplings in the indirect dimension. The experimental C^α and CO resonances for two representative residues are shown in Fig. 4b. The ^{13}C' spectrum shown in the center of the Figure is extracted from a ^{13}C detected HNCO correlation which was recorded for comparison using the pulse scheme represented in Fig. 1d. In uniformly labeled proteins, a potentially favourable natural ^{13}C line width can only be exploited if all ^{13}C,^{13}C scalar couplings are refocused effectively during the respective evolution period. Efficient homonuclear decoupling is readily achieved in indirect evolution periods involving carbonyl resonances. In contrast, ^{13}C detection in the direct dimension yields broad lines due to the evolution of homonuclear scalar couplings. Decoupling can here in principle be achieved using spin state selective experiments (Duma et al. 2003; Laage et al. 2009), by application of homonuclear decoupling in the direct dimension (Chevelkov et al. 2005) or by processing the data using *J*-deconvolution (Agarwal et al. 2009). These techniques, however, usually compromise the sensitivity of the experiment. Effective homonuclear decoupling in the C^α indirect dimension in a HNCA correlation is difficult given the poor separation of the C^α and C^β resonances. Use of a constant-time element (Chen et al. 2007; Yamazaki et al. 1994) in the pulse sequence overcomes this issue. However, sensitivity is significantly

Fig. 2 Strip plots from a MAS solid-state NMR HNCACO experiment yielding sequential H^N, N^H, and CO_{i-1} as well as intraresidual H^N, N^H, and CO_i connectivities between residues L8 and K18 in the α-spectrin SH3 domain (*black contour lines*). The spectra are superimposed with HNCO strip plots, which exclusively contain H^N, N^H, and CO_{i-1} correlations (*red contour lines*). The 3D-HNCACO was recorded within 3 days using a t_1^{max} of 20 ms
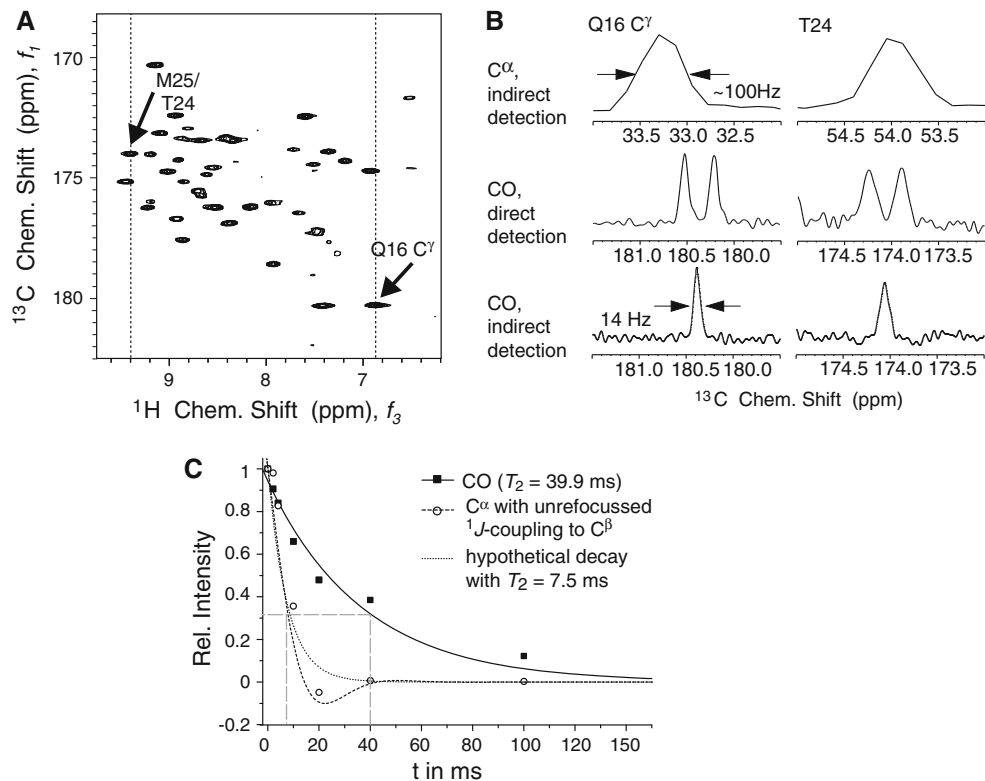
Fig. 4 **a** First 2D ^{13}CO,$^{1}H^N$ plane of the 3D MAS solid-state HNCO experiment, showing the favourable dispersion of the CO chemical shifts for the α-spectrin SH3 domain. **b** 1D traces extracted from a typical solid-state HNCA (only $C^α$,CO decoupling, top) and HNCO experiment recorded without (^{13}C detection, center) and with ^{13}CO,$^{13}C^α$ decoupling (^{1}H detection, bottom), respectively. The frequency axes of the 1D spectra are plotted to the same scale in the $^{13}C^α$ and CO spectral region. The HNCA and HNCO were acquired using a t_1^{max} of 9 and 100 ms, respectively. No apodization was used in the CO dimensions. **c** Signal decay during an indirect carbon evolution period. The *solid line* (*black squares*) represents CO transverse magnetization (with $^{13}C^α$,^{13}CO decoupling), while the *dashed line* (*open circles*) refers to $C^α$ (with $^{13}C^α$,^{13}CO and ^{2}H,$^{13}C^α$ decoupling). $^{1}J_{C^αC^β}$ can not be efficiently refocused due to overlap of $C^α$ and $C^β$ chemical shifts. This results in a fast signal decay. The effective line width corresponds to an apparent T_2^{app} of ∼7.5 ms. In case ^{2}H,^{13}C scalar couplings are not refocused, the apparent decay is even faster

compromised due to the length of the constant time period. In case standard triple-resonance probes are employed, $C^α$ resonances are slightly broadened due to evolution of scalar couplings to ^{2}H. In the future, quadruple resonance probes that have an additional channel for ^{2}H will allow to overcome this problem.

In order to put the achievable resolution in the solid-state in context, we compared the experimental line width obtained here with the line width expected in solution. In solution, molecular tumbling can compromise sensitivity and resolution depending on the molecular weight of the dissolved protein. The transverse relaxation rates $R_2 = 1/T_2$ crucially depend on the correlation time $τ_c$ of rotational diffusion, which increases for proteins with increasing molecular weight (Dayie and Wagner 1997; Lee et al. 2006). Even though there are examples of investigations on large protein complexes (Tugarinov et al. 2002; Tugarinov et al. 2009), solution-state NMR is inherently linked to small or intermediate sized molecules. In general, transverse relaxation of carbonyl carbons in a protein is

dominated by chemical shift anisotropy (CSA). The respective relaxation rate $R_{2,CSA}$ is given as (Dayie and Wagner 1997)

$$R_{2,CSA} = (d_{CSA}^2 ω_C^2/6)[4J_{C'}(0) + 3J_{C'}(ω_C)],$$

with a generalized CSA coupling constant $d_{CSA}^2 = (1/3) Δδ^2[1 + η^2/3] = 6.2 × 10^{-9}$, (Engelke and Rüterjans 1997), where $Δδ$ and $η$ represent the anisotropy and the asymmetry of the CSA tensor, respectively. $J_{C'}(ω)$ refers to the spectral density function at frequency $ω$.

A calculation of the expected ^{13}CO relaxation rates in solution at 14.1 T (corresponding to a ^{1}H Larmor frequency of 600 MHz) is shown in Fig. 5, together with the experimental solid-state decay rate (Fig. 4c). For illustration, solution-state correlation times for ubiquitin, the CDK inhibitor p19[INK4d], malate synthase G and the "half proteasome", are drawn into the figure (Renner et al. 1998; Tjandra et al. 1995; Tugarinov et al. 2002, 2009). The simulation of the solution-state $^{13}C'$ relaxation rates assume order parameters S^2 of 0.8 and 1.0, respectively
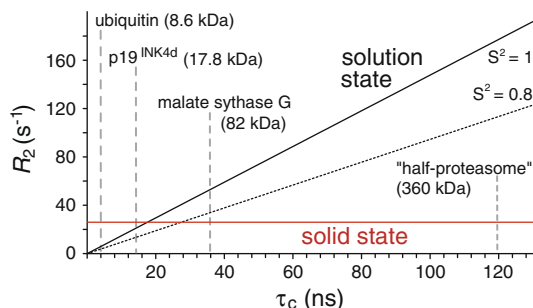
Fig. 5 Carbonyl transverse relaxation rates R_2 in solution and in the solid state. Whereas R_2 in solution (*black*) strongly depends on the correlation time τ_c, the line width in the solid-state is molecular weight independent. For the micro-crystalline SH3 domain, we find a value of 25 s^{-1} ($T_2 = 40$ ms, *red*). The *dashed black line* shows ^{13}CO relaxation rates in solution assuming a generalized order parameter S^2 of 0.8, while the solid black line is obtained assuming an order parameter of one. *Vertical*, *dashed lines* indicate typical values for the motional correlation time τ_c for several proteins in solution. The calculation was carried out assuming an external magnetic field of 14.1 T (600 MHz)

(Engelke and Rüterjans 1997). For intermediate or large proteins, the plot shows that the carbonyl resonance line width in the solid-state can potentially be smaller than the line width obtainable in solution. The break-even is reached for motional correlation times of $\tau_C \sim 25$ ns.

The comparison given above assumes that the origin of line widths are sample homogeneity, residual homo- and heteronuclear dipolar couplings which are due to insufficient MAS rotation frequencies and decoupling, respectively, MA missetting and relaxation due to local dynamics. Other sources might involve the anisotropic magnetic susceptibility (Cowans and Grutzner 1993; Garroway 1977; Vanderhart et al. 1981). The estimated molecular weight at which solid-state NMR yields a more favourable resolution compared to solution-state NMR experiments therefore represents an upper limit that is implied by the current technology. We expect that with improved sample preparation and the availability of faster MAS rotation frequencies, the break-even should rather be shifted towards lower molecular weights.

Conclusion

We have shown that solid-state NMR of extensively deuterated proteins yields excellent resolution in the ^{1}H, ^{15}N, and ^{13}C dimension. We find carbonyl line widths which are on the order of 14–17 Hz. This makes the C' dimension—similar as in solution-state NMR—attractive for CO-based sequential backbone assignment using HNCO/HNCACO experiments. Whereas in solution, relaxation increases with increasing molecular weight, the line width in the solid state is independent of tumbling and thus on the molecular

weight. A break-even in resolution compared to solution-state NMR is achieved for proteins with a molecular weight on the order of $\tau_C \sim 25$ ns (corresponding to proteins with ~ 30 kDa). The fact that resolution does not depend on the molecular weight in the solid-state should pave the way for NMR investigations of large nanocrystalline proteins. We expect that high resolution spectra based on magnetization transfer schemes employing scalar couplings and proton detection will find widespread use, as high MAS speeds are becoming routinely available.

References

Agarwal V, Faelber K, Schmieder P, Reif B (2009) High-resolution double-quantum deuterium magic angle spinning solid-state NMR spectroscopy of perdeuterated proteins. J Am Chem Soc 131:2–3

Akbey Ü, Lange S, Franks WT, Linser R, Rehbein K, Diehl A, van Rossum B-J, Reif B, Oschkinat H (2009) Optimum levels of exchangeable protons in perdeuterated proteins for proton detection in MAS solid-state NMR spectroscopy. J Biomol NMR 46:67–73

Baldus M (2002) Correlation experiments for assignment and structure elucidation of immobilized polypeptides under magic angle spinning. Prog Nucl Magn Reson Spectrosc 41:1–47

Chen L, Kaiser JM, Polenova T, Yang J, Rienstra CM, Mueller LJ (2007) Backbone assignments in solid-state proteins using J-based 3D heteronuclear correlation spectroscopy. J Am Chem Soc 129:10650–10651

Chevelkov V, Chen Z, Bermel W, Reif B (2005) Resolution enhancement in MAS solid-state NMR by application of 13C homonuclear scalar decoupling during acquisition. J Magn Reson 172:56–62

Chevelkov V, Rehbein K, Diel A, Reif B (2006) Ultra-high resolution in proton solid-state NMR spectroscopy at high levels of deuteration. Angew Chem Int Ed 45:1–5

Chevelkov V, Faelber K, Schrey A, Rehbein K, Diehl A, Reif B (2007) Differential line broadening in MAS solid-state NMR due to dynamic interference. J Am Chem Soc 129:10195–10200

Clubb RT, Thanabal V, Wagner G (1992) A constant-time three-dimensional triple-resonance pulse scheme to correlate intraresidue 1HN, 15N, and 13CO chemical shifts in 15N–13C-labeled proteins. J Magn Reson 97:213–217

Cowans BA, Grutzner JB (1993) Examination of homogeneous broadening in solids via rotationally synchronized spin-echo NMR-spectroscopy. J Magn Reson Ser A 105:10–18

Dayie KT, Wagner G (1997) Carbonyl carbon probe of local mobility in 13C, 15N-enriched proteins using high-resolution nuclear magnetic resonance. J Am Chem Soc 119:7797–7806

Duma L, Hediger S, Brutscher B, Böckmann A, Emsley L (2003) Resolution enhancement in multidimensional solid-state NMR spectroscopy of proteins using spin-state selection. J Am Chem Soc 125:11816–11817

Emsley L, Bodenhausen G (1989) Self-refocusing effect of 270° gaussian pulses. Applications to selective two-dimensional exchange spectroscopy. J Magn Reson 82:211–221

Emsley L, Bodenhausen G (1990) Gaussian pulse cascades: new analytical functions for rectangular selective inversion and in-phase excitation in NMR. Chem Phys Lett 165:469–476

Engelke J, Rüterjans H (1995) Sequential protein backbone resonance assignments using an improved 3D-HN(CA)CO pulse scheme. J Magn Reson B 109:318–322

Engelke J, Rüterjans H (1997) Backbone dynamics of proteins derived from carbonyl carbon relaxation times at 500, 600 and 800 MHz: application to ribonuclease T1. J Biomol NMR 9:63–78

Garroway AN (1977) Homogeneous and inhomogeneous nuclear spin echoes in organic solids: adamantane. J Magn Reson 28:365–371

Goddard TD, Kneller DG SPARKY 3. University of California, San Francisco

Laage S, Lesage A, Emsley L, Bertini I, Felli IC, Pierattelli R, Pintacuda G (2009) Transverse-dephasing optimized homonuclear J-decoupling in solid-state NMR spectroscopy of uniformly 13C-labeled proteins. J Am Chem Soc 131:10816–10817

Lange A, Becker S, Seidel K, Giller K, Pongs O, Baldus M (2006) A concept for rapid protein-structure determination by solid-state NMR spectroscopy. Angew Chem Int Ed 44:2089–2092

Lee D, Hilty C, Wider G, Wüthrich K (2006) Effective rotational correlation times of proteins from NMR relaxation interference. J Magn Reson 176:72–76

Linser R, Chevelkov V, Diehl A, Reif B (2007) Sensitivity enhancement using paramagnetic relaxation in MAS solid-state NMR of perdeuterated proteins. J Magn Reson 189:209–216

Linser R, Fink U, Reif B (2008) Proton-detected scalar coupling based assignment strategies in MAS solid-state NMR spectroscopy applied to perdeuterated proteins. J Magn Reson 193:89–93

Linser R, Fink U, Reif B (2009) Probing surface accessibility of proteins using paramagnetic relaxation in solid-state NMR spectroscopy. J Am Chem Soc 131:13703–13708

Mainz A, Jehle S, van Rossum B-J, Oschkinat H, Reif B (2009) Large protein complexes with extreme rotational correlation times investigated in solution by magic-angle-spinning NMR spectroscopy. J Am Chem Soc 131:15968–15969

Pauli J, Baldus M, van Rossum B, de Groot H, Oschkinat H (2001) Backbone and side-chain 13C and 15N signal assignments of the α-spectrin SH3 domain by magic angle spinning solid-state NMR at 17.6 tesla. ChemBioChem 2:272–281

Renner C, Baumgartner R, Noegel AA, Holak TA (1998) Backbone dynamics of the CDK Inhibitor p19INK4d studied by ^{15}N NMR relaxation experiments at two field strengths. J Mol Biol 283:221–229

Schanda P, Huber M, Verel R, Ernst M, Meier BH (2009) Direct detection of $^{3h}J_{NC'}$ hydrogen-bond scalar couplings in proteins by solid-state NMR spectroscopy. Angew Chem Int Ed 48:9322–9325

Shaka AJ, Keeler J, Frenkiel T, Freeman R (1983) An improved sequence for broadband decoupling: WALTZ-16. J Magn Reson 52:335–338

Tian Y, Chen L, Niks D, Kaiser JM, Lai J, Rienstra CM, Dunn MF, Mueller LJ (2009) J-Based 3D sidechain correlation in solid-state proteins. Phys Chem Chem Phys 11:7078–7086

Tjandra N, Feller SE, Pastor RW, Bax A (1995) Rotational diffusion anisotropy of human ubiquitin from 15N NMR relaxation. J Am Chem Soc 117:12562–12566

Tugarinov V, Muhandiram R, Ayed A, Kay LE (2002) Four-dimensional NMR spectroscopy of a 723-residue protein: chemical shift assignments and secondary structure of malate synthase G. J Am Chem Soc 124:10025–10035

Tugarinov V, Sprangers R, Kay LE (2009) Probing side-chain dynamics in the proteasome by relaxation violated coherence transfer NMR spectroscopy. J Am Chem Soc 129:1743–1750

Vanderhart DL, Earl WL, Garroway AN (1981) Resolution in C-13 NMR of organic-solids using high-power proton decoupling and magic-angle sample spinning. J Magn Reson 44:361–401

Wasmer C, Lange A, Melckebeke Hv, Siemer AB, Riek R, Meier BH (2008) Amyloid fibrils of the HET-s(218–289) prion form a beta solenoid with a triangular hydrophobic core. Science 319:1523–1526

Yamazaki T, Lee W, Revington M, Mattiello DL, Dahlquist FW, Arrowsmith CH, Kay LE (1994) An HNCA pulse scheme for the backbone assignment of 15 N,13C,2H-labeled proteins: application to a 37-kDa Trp repressor-DNA complex. J Am Chem Soc 116:6464–6465

Zhou DH, Shea JJ, Nieuwkoop AJ, Franks WT, Wylie BJ, Mullen C, Sandoz D, Rienstra CM (2007) Solid-state protein structure determination with proton-detected triple resonance 3D magic-angle spinning NMR spectroscopy. Angew Chem Int Ed 46:8380–8383